Synsint Research Group

Available online at www.synsint.com

Synthesis and Sintering

ISSN 2564-0186 (Print), **ISSN** 2564-0194 (Online)

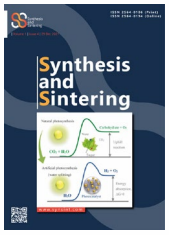

Research article

Microstructure and mechanical properties of Ti_3SiC_2 MAX phases sintered by hot pressing

Sheida Haji Amiri *, Nasser Pourmohammadie Vafa

Department of Materials Science and Engineering, University of Tabriz, Tabriz, Iran

ABSTRACT

This study aimed to investigate the effect of sintering temperature on Ti_3SiC_2 samples' microstructure and mechanical properties, including three-point flexural strength, Vickers hardness, and fracture toughness. Therefore, Ti_3SiC_2 samples were sintered under a vacuum atmosphere at a pressure of 35 MPa for 30 minutes at two temperatures of 1500 and 1550 °C by hot pressing. The microstructure obtained from the fracture cross-section of the samples shows that by increasing the sintering temperature to 1550 °C the microstructure of this sample becomes larger than the sintered sample at 1500 °C. Also, increasing the sintering temperature to 1550 °C causes the decomposition of Ti_3SiC_2 to TiC, which can be seen in the X-ray diffraction pattern (XRD). In addition, the relative density of the sintered sample at 1550 °C is 98.08% which is higher than that of the sintered sample at 1500 °C with the result of 89%. On the other hand, the three-point flexural strength (227.5 MPa), the Vickers hardness (~9 GPa), and the fracture toughness (8.6 MPa.$m^{1/2}$) of the sintered sample at 1500 °C are higher due to the fine-grained structure.

KEYWORDS

MAX phase
Ti_3SiC_2
Hot pressing
Microstructure
Mechanical properties

OPEN ACCESS

1. Introduction

The MAX phases are a group of ternary (i.e., consisting of three elements) compounds with the family formula: $M_{N+1}AX_N$; where M is early transition metal; N is a round number 1, 2, or 3; A is an element from groups mostly IIIA and IVA in the periodic table of the elements and X is either nitrogen or carbon [1, 2]. MAX phases are divided into classes according to the value of N, and Ti_3SiC_2 belongs to class 312. There are three classes of MAX phases; the other two are 211 and 413, with N values of 1 and 3 [3]. MAX phases have attracted much attention recently [4]. Electrically, thermally and elastically, the MAX phases share many of the advantageous attributes of their respective binary metal carbides or nitrides: they are thermally and electrically conductive and elastically stiff [3, 5]. They have a high stiffness [6]. Their layered structure achieves the MAX phase's characteristic and unusual combination of mechanical properties [7]. The bonds within the nitride or carbide layers are very strong, while the bonds between the layers are weaker and allow for basal slip and dislocation [3]. MAX phases combine some advantages of ceramic and metal, and the ternary compounds have an abrasion-resistant layer that can be machined and do not become brittle [8–10]. Recently, Ti_3SiC_2 has been of practical interest because of its unique and excellent combination of physical and mechanical properties such as relatively low hardness (H_V 4 GPa), high electrical (4.5×10^6 $\Omega^{-1}m^{-1}$) and thermal conductivities (40 W/m.k) which is twice that of titanium metal [11–14], excellent oxidation resistance, thermal shock resistance, high melting point (3000 °C), high damage tolerance, machinability, high stability at high temperatures, relatively low density (4.53 g/cm^3), high elastic modulus and strength, and a high ratio of fracture toughness to strength, also self-lubricating properties [4, 15–19]. In addition, the specific stiffness of Ti_3SiC_2 is roughly three times that of titanium metal [20–24]. Also Ti_3SiC_2 and TiC have similar bonding environment as both of them share Ti-C covalent bond and due to that, Ti_3SiC_2 shares many of the properties of their corresponding binary carbide, TiC [25]. These properties have

* Corresponding author. *E-mail address:* sh_hajiamiri@tabrizu.ac.ir (S. Haji Amiri)

Received 22 November 2021; Received in revised form 26 December 2021; Accepted 27 December 2021.

https://doi.org/10.53063/synsint.2021.1472

made the MAX phases good candidates for the replacement of high-temperature ceramics and metals in the industries [26]. It is mainly used as corrosion and wear protective material, high-temperature structural materials, batteries and heat exchangers, etc. [6]. Also this different classification of properties makes Ti_3SiC_2 a promising material especially for high temperature applications [27] and many important industrial applications [28] such as engine cylinders and jet engines, electrical contacts, turbine blades, Severe environment like in spacecraft [25]. The crystalline structure of Ti_3SiC_2 is composed of hexagonal lattices of Si atoms separated by three closely spaced Ti layers, which place the C atoms in octagonal positions [29, 30]. Therefore, it is important to make high purity and fully dense bulk Ti_3SiC_2 samples. Zhou et al. [31] were the first who synthesize the ternary compound via a chemical reaction between Si, graphite, and TiH_2, at 2000 ºC, followed by the work of Nickl et al. [32] by using the chemical vapour deposition (CVD) method. During the last decade, different methods have been used to synthesize bulk Ti_3SiC_2, such as hot isostatic pressing (HIP), reactive sintering, arc melting, hot pressing (HP), and others. However, the synthesis process of all these techniques involves high temperature and pressure or is much time-consuming [33, 34]. Due to the presence of impurity phases in the purchased ready-made Ti_3SiC_2 powder according to the relevant X-ray diffraction pattern, the aim of this study is to investigate the effect of different temperatures with a difference of 50 °C on the hot-pressed monolithic Ti_3SiC_2 samples and the formed phases, microstructure and mechanical properties, to see at which sintering temperature the impurity phases disappear or reach their minimum value. The sample's microstructure, mechanical and physical behavior produced by different analytical techniques such as XRD, SEM, three-point flexural strength, Vickers hardness, and fracture toughness tests were investigated.

2. Experimental

2.1. Sample preparation

In this research, purchased ready-made Ti_3SiC_2 (average particle size : ≤ 15 µm; Xi'AN BIOF BIO-TECH Co. Ltd.) was used as starting material. Before sintering, the X-ray diffraction pattern and SEM micrographs of the purchased ready-made Ti_3SiC_2 powder with 2 different magnifications are shown in Fig. 1. The X-ray diffraction pattern of the Ti_3SiC_2 powder indicates that, the main peak at an approximate position of 41 ° corresponds to the Ti_3SiC_2 and Ti phases. In addition to the main phases, the TiC phase is seen in the pattern. Also, the unreacted C and Si elements beside to the TiSi phase were detected in the pattern as impurity phases. The reason for the existence of such phases can be attributed to the imperfection of chemical reactions and the synthesis process as well as the low temperature of the process. For this purpose, in order to remove impure phases including TiC, C and Si, the purchased MAX phase powder was sintered at two different temperatures and the results were investigated. Also SEM images of Ti_3SiC_2 MAX phase powder show the layered structure of this compound along with the impure phases observed in the XRD pattern of this sample.

To get rid of impure phases, the sample for comparison in 2 different temperatures was hot-pressed. For the hot pressing process, Ti_3SiC_2 powder was poured into graphite cylindrical molds measuring 25×10×10 mm^3. Because most of the MAX phase powder melts and

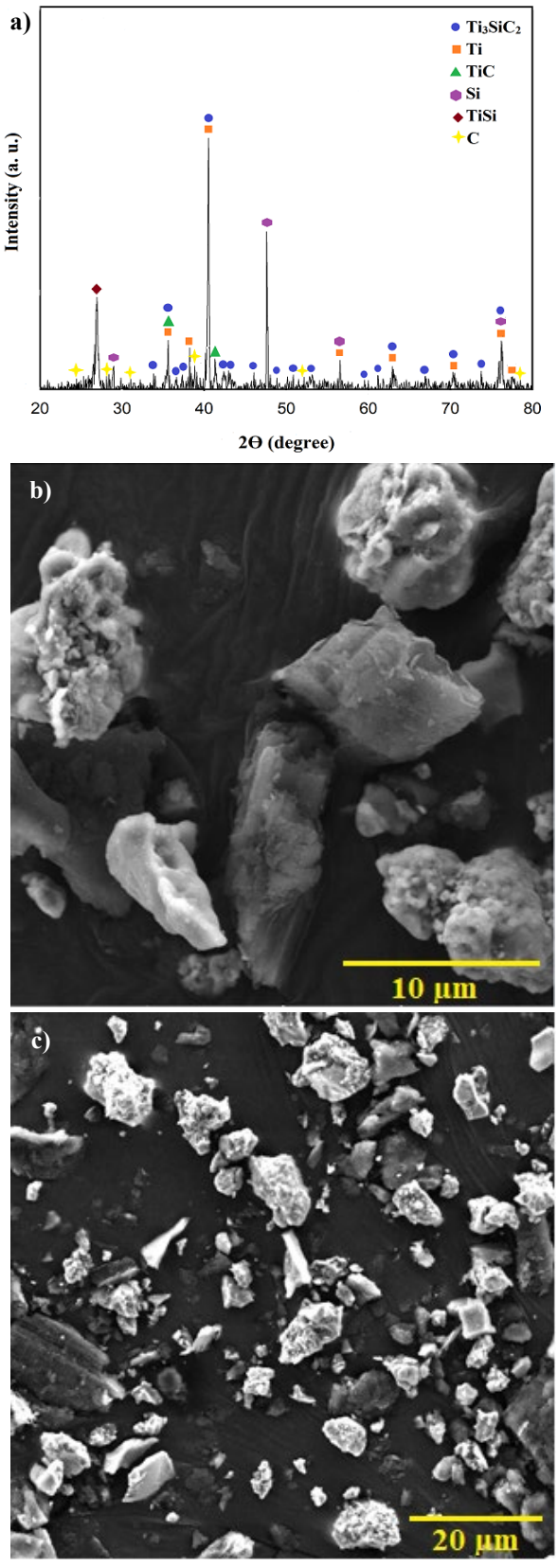

Fig. 1. a) X-ray diffraction pattern and b, c) SEM micrographs of as-purchased Ti_3SiC_2 powder in two different magnifications.

reacts with the graphite mold, to prevent the adhesion of the mold surfaces and the produced samples, we used graphite sheets with a thickness of 0.2 mm to easily remove the samples from the mold, and also we used boron nitride (BN) with a grain size of about 2 µm due to its neutrality and lubricating properties. Finally, thin pieces of graphite sheets with suitable dimensions were used to cover the surfaces in contact with the punch. The hot pressing process was performed at 1500 °C and 1550 °C for 30 minutes in a vacuum chamber (5×10^{-2} Pa) at a pressure of about 35 MPa. At the end of the process, the heating system was turned off, and the furnace was cooled to room temperature. The surfaces of the samples were then ground with SiC sandpaper, then polished with diamond paste, and then ultrasonically cleaned in a distilled water bath and air-dried.

2.2. Characterization of the samples

The phase analysis of the hot-pressed samples was performed by a Bruker advanced D8 X-ray diffractometer with the following specifications: Cu lamp, λ = 1.54 Å, 40 kV, 40 mA, and step size of 20 degree. The XRD spectra were analyzed by the X'Pert High Score Plus package. A TESCAN field emission scanning electron microscope was employed to study the microstructure of the specimens. Chemical analysis of the elements was performed by energy dispersive spectroscopy (Digital X-Ray Processor: DXP-X10P). The Archimedes method was applied to measure the bulk density of the samples, using distilled water as the immersing medium, according to the ASTM C20 standard. The relative density was calculated using Eq. 1:

$$RD = \frac{\rho_b}{\rho_t} \times 100 \quad (1)$$

where RD is the relative density, ρ_b is the bulk density, and ρ_t is the theoretical density. The rule of mixtures was used to estimate the theoretical density of samples. The porosity of the samples was calculated according to Eq. 2:

$$P = 100 - RD \quad (2)$$

where P is the percentage of porosity in the hot-pressed samples.
The samples with the dimension of $25\times4\times3$ mm^3 were first cut from the primary samples to study the mechanical properties of the manufactured specimens. Then, the sliced samples were ground and polished with diamond paste, and the three-point flexural strength test (Zwick Roell) was performed according to ASTM C1161 standard. The three-point flexural strength was evaluated by Eq. 3:

$$S = \frac{3}{2}\frac{PL}{bh^2} \quad (3)$$

where S is the three-point flexural strength (MPa), h is the height (mm), P is the applied load (N), and b is the width of the sample (mm), L is the bearing distance that is 20 mm, and the loading rate is 0.1 mm/min. Five samples were tested for each sample to measure the three-point flexural strength. Also, the Vickers hardness of the specimens was measured using a 50 N indentation load and a 20 s dwell time (SCTMC HV-1000Z) as given in Eq. 4, according to ASTM E92 standard:

$$H_v = 1.854\frac{P}{d^2} \quad (4)$$

where H_V is Vickers hardness, d is the average length of the diagonal left by the indenter, and P is the applied load. Each expressed magnitude of Vickers hardness has been repeated an average of 8 times.

The fracture toughness of the samples was obtained by direct measurement of induced crack length (by indentation technique). After measuring Vickers hardness by depressions on polished surfaces, the fracture toughness of the samples was calculated. If the recess force is sufficient, radial cracks will form in the corners of the recess molds. By measuring the length of the cracks by light microscopy (Eclips MA10), the fracture toughness of the samples was obtained using the Eq. 5:

$$K_{IC} = 0.016\left(\frac{E}{H_v}\right)^{0.5}\left(\frac{P}{C^{1.5}}\right) \quad (5)$$

where K_{IC} is fracture toughness, H_V is Vickers hardness, E is elastic modulus, P is indentation load, and C is the mean length of cracks.
The grain thickness of the samples was calculated by ImageJ software (version 1.44) with the help of SEM micrographs of the samples.

3. Results and discussion

The XRD spectra of the hot-pressed monolithic Ti_3SiC_2 specimens at 1500 °C and 1550 °C are shown in Fig. 2. According to Fig. 2, only the Ti_3SiC_2, TiC, and $TiSi_2$ phases were identified in the XRD pattern of the hot-pressed Ti_3SiC_2 sample at 1500 °C. In the hot-pressed Ti_3SiC_2 sample at 1550 °C, the Ti_3SiC_2 and TiC phases were identified in the XRD pattern. In the Ti_3SiC_2 sample sintered at 1500 °C, Ti_3SiC_2 phase was as the main phase, but in the Ti_3SiC_2 sample sintered at 1550 °C, the TiC phase is identified as the main phase which has been attributed

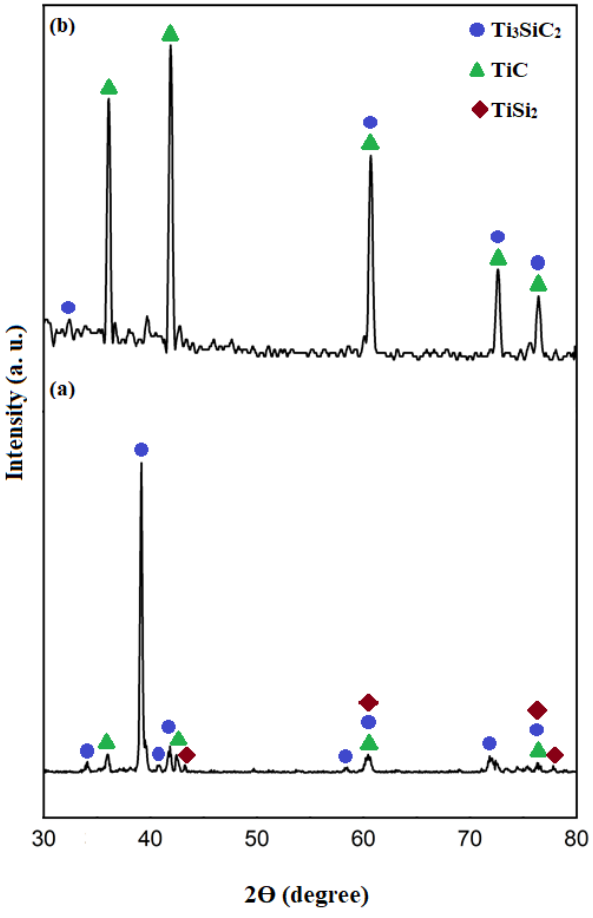

Fig. 2. X-ray diffraction patterns of Ti_3SiC_2 specimens hot-pressed at a) 1500 °C and b) 1550 °C.

to the decomposition of Ti_3SiC_2 during hot pressing due to the weak resistance of Ti_3SiC_2 against carburization (see Eq. 6) [35–37].

$$Ti_3SiC_2 + (3x-1)C = 3TiC_x + SiC \quad (6)$$

The presently reported data show that Ti_3SiC_2 is thermally stable up to about 1500 °C. Above this temperature, it withstands a decomposition and the kinetics is highly relevant on the nature of the environment which surrounds Ti_3SiC_2. A graphite crucible seems to begin the decomposition process, resulting in a decomposition threshold temperature 50 °C more than for an alumina crucible, in which Ti_3SiC_2 is stable up to about 1450 °C and then is decomposed very slowly. The following reaction can be responsible for the decomposition of Ti_3SiC_2 (see Eq. 7) [38]:

$$Ti_3SiC_2(s) = 3TiC_x(s) + Si(g), \Delta G = 181 \text{ KJ/mol} \quad (7)$$

In the environment around graphite, Eq. 7 can lead to the formation of SiC, according to the following equation (see Eq. 8):

$$Si(g) + C = SiC, \Delta G = -276 \text{ KJ/mol} \quad (8)$$

Comparing Figs. 1 and 2, it is seen that the free Si, C and Ti elements react together to form the Ti_3SiC_2 and $TiSi_2$ intermediate phases. The TiC phase with low-intensity is also present in the sintered Ti_3SiC_2 MAX phase sample at 1500 °C, and with high-intensity (main peak) is seen in the sintered samples at 1550 °C. This decrease and increase for the intensity of TiC phase can be attributed to the reaction of this substance with Si for achieving the Ti_3SiC_2 phase and partial decomposition of the Ti_3SiC_2 phase at high temperatures according to Eq. 6.

Scanning electron microscopy (SEM) was used to study the fracture surface of the hot-pressed monolithic Ti_3SiC_2 specimens at two different temperatures with two different magnifications (Fig. 3). As can be seen from the micrographs, in the hot-pressed Ti_3SiC_2 sample at 1500 °C, Ti_3SiC_2 grains with the elongated and layered structure were identified, and based on the XRD pattern of this sample, the impure phases of TiC and $TiSi_2$, respectively Light gray and dark gray particles are mainly distributed in Ti_3SiC_2 grain boundaries and inhibit the growth of Ti_3SiC_2 granules of a, b. Also, in the hot-pressed Ti_3SiC_2 sample at 1550 °C c, d, layered and elongated Ti_3SiC_2 particles along with light gray TiC particles are visible in the microstructure. The only difference in the microstructure of the two samples is the limited placement of TiC particles in the grain boundaries of hot-pressed Ti_3SiC_2 particles at 1550 °C, which causes the growth of Ti_3SiC_2 particle grains. The grain thickness of the samples is reported in Table 1. It is also worth noting that in both monolithic specimens, both transgranular and intergranular fractures were observed. The fracture mode of Ti_3SiC_2 grains includes partial intergranular fracture leading to

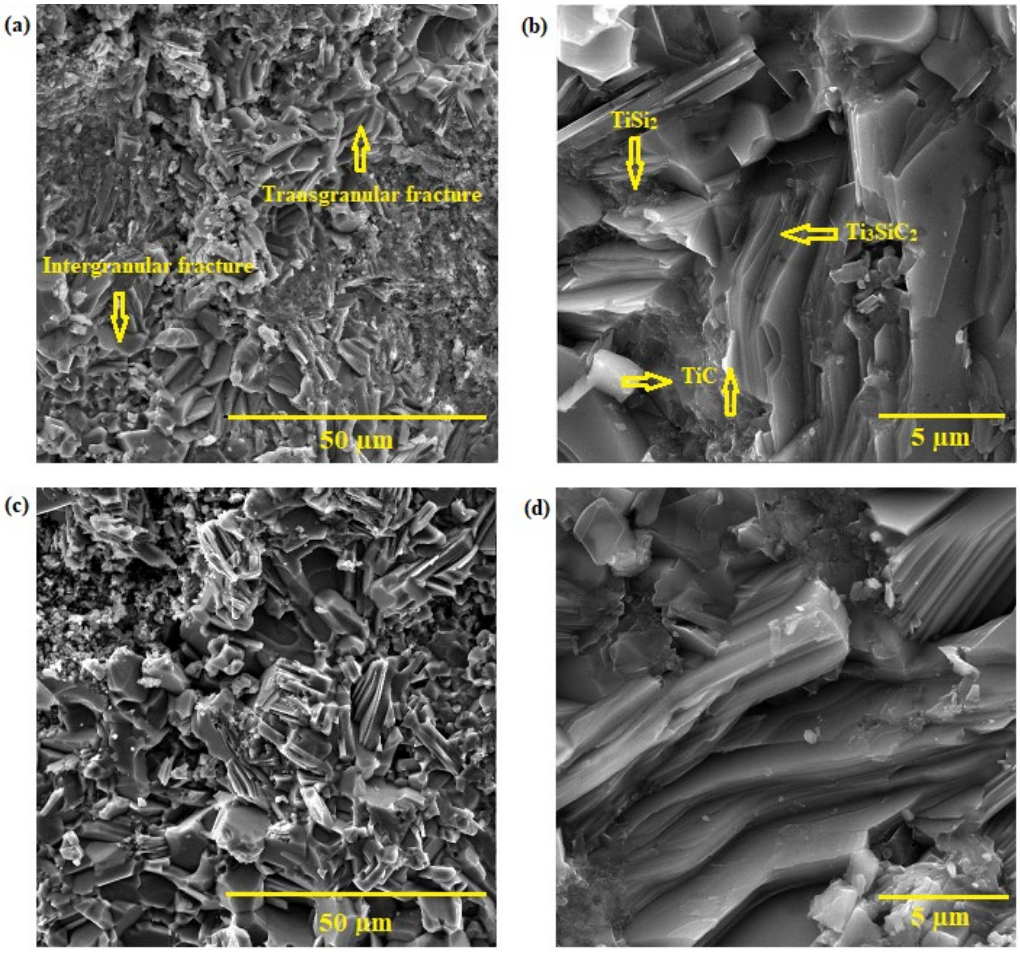

Fig. 3. SEM images of Ti_3SiC_2 specimens hot-pressed at a, b) 1500 °C and c, d) 1550 °C.

Table 1. Particle thickness of as-received Ti_3SiC_2 material and grain thickness of hot-pressed Ti_3SiC_2 specimens.

Sample	Thickness (μm)
Ti_3SiC_2 powder	1.24 ± 0.31
Ti_3SiC_2 hot-pressed at 1500 °C	1.26 ± 0.68
Ti_3SiC_2 hot-pressed at 1550 °C	1.36 ± 0.85

integrated layer microstructure and partial transgranular fracture indicating cleavages in the sample [14]. The presence of these two failure modes indicates the existence of phases with different hardness. Similar failure modes were observed in the formation of Ti_3SiC_2 reported by Abderrazak et al. [28].

Bulk and relative density together with total, apparent, and closed porosity values of the hot-pressed Ti_3SiC_2 samples at 1500 °C and 1550 °C are presented in Table 2. Hot-pressed Ti_3SiC_2 at 1550 °C has a higher density than the sample hot-pressed Ti_3SiC_2 at 1500 °C. Due to the decomposition of the sintered Ti_3SiC_2 sample at 1550 °C to the TiC phase as the main peak with a theoretical density of 4.91 g/cm^3 [39], the density of the sintered Ti_3SiC_2 sample at 1550 °C increased compared to the sintered Ti_3SiC_2 sample at 1500 °C. In contrast, the hot-pressed Ti_3SiC_2 sample at 1500 °C has a lower density than the hot-pressed Ti_3SiC_2 sample at 1550 °C due to the formation of minor TiC phases with a theoretical density of 4.91 g/cm^3 and $TiSi_2$ with a theoretical density of 4.02 g/cm^3. Also, the decrease in density of hot-pressed Ti_3SiC_2 sample at 1500 °C compared to hot-pressed sample at 1550 °C can be attributed to sintering conditions such as relatively low reaction temperature [33, 40].

The three-point flexural strength of the monolithic Ti_3SiC_2 samples produced at two different temperatures was investigated (Fig. 4). According to this figure, the three-point flexural strength of the hot-pressed monolithic Ti_3SiC_2 specimen at 1500 °C was 227.5 MPa. While the three-point flexural strength of the hot-pressed monolithic Ti_3SiC_2 specimen at 1550 °C was 179.9 MPa. The three-point flexural strength of the ternary layered compound Ti_3SiC_2 is 260–600 MPa [17, 25]. According to the X-ray diffraction pattern of both hot-pressed samples at 1500 °C and 1550 °C, the TiC phase is formed in both samples, while in the hot-pressed sample at 1550 °C is seen as the main peak resulting from the partial decomposition of Ti_3SiC_2 and is dominant over Ti_3SiC_2, due to the mismatch of the coefficient of thermal expansion between Ti_3SiC_2 (9.7×10^{-6}/K along c-direction and 8.6×10^{-6}/K along a-direction) and TiC (7.4×10^{-6}/K) [25, 41], the three-point flexural strength of the sintered Ti_3SiC_2 specimen at 1550 °C decreased compared to the sintered specimen at 1500 °C. Besides that, according to the images obtained from scanning electron microscopy and reported grain thicknesses in Table 1, the TiC and $TiSi_2$ phases formed in the hot-pressed Ti_3SiC_2 sample at 1500 °C compared to the hot-pressed Ti_3SiC_2 sample at 1550 °C are located in the grain boundaries and prevents the growth of Ti_3SiC_2 grains compared to the hot-pressed sample at 1550 °C. Due to the Hall-Petch effect and the inverse relationship between grain size and strength, it causes an increase in the three-point flexural strength of this sample compared to the hot-pressed sample at 1550 °C. On the other hand, increasing the sintering temperature to 1550 °C causes grain growth and decreases the three-point flexural strength. Also, the three-point flexural strength of both specimens decrease compared to the Ti_3SiC_2 MAX phase which could be the result of an increase in grain thickness of both sintered samples compared to Ti_3SiC_2 MAX phase [27].

Vickers hardness values of the hot-pressed monolithic Ti_3SiC_2 samples at 1500 °C and 1550 °C are shown in Fig. 5. The hardness values measured in this study are higher than the values reported for the monolithic Ti_3SiC_2 MAX phase (~4 GB) [17]. In the hot-pressed Ti_3SiC_2 sample at 1500°C, due to the formation of the TiC and $TiSi_2$ phases in the sample and the high hardness of the TiC phases (28–35 GPa) [41] as well as the $TiSi_2$ phase (~8 GPa) [42], and also due to the high three-point flexural strength of this specimen, the hardness of this sample is high (~ 9 GPa). In the case of the hot-pressed Ti_3SiC_2 sample at 1550 °C, hardness of 7.1 GPa has been reported, which according to the corresponding X-ray diffraction pattern, is attributed to the presence of TiC in the sample as the main peak resulting from the decomposition of Ti_3SiC_2 at 1550 °C. By increasing the temperature, also there is high TiC particles in this sample but grain growth over comes to the high hardness of TiC particles (28–35 GPa) and causes the decrease in the hardness.

Fig. 6. shows the fracture toughness of the hot-pressed monolithic Ti_3SiC_2 samples at 1500 °C and 1550 °C. As you can see, the fracture toughness for the hot-pressed Ti_3SiC_2 sample at 1500 °C is 8.6 MPa.m$^{1/2}$ and for the hot-pressed Ti_3SiC_2 sample at 1550 °C equal to 7.8 MPa.m$^{1/2}$ which are in the range of the value reported for the Ti_3SiC_2 MAX phase sample (6–11 MPa.m$^{1/2}$) [17]. One of the main reasons for the increase in fracture toughness of the sintered Ti_3SiC_2 sample at 1500 °C compared to the sintered sample at 1550 °C can be attributed to the presence of TiC and $TiSi_2$ particles in the Ti_3SiC_2 grain boundaries and the formation of fine grain structure which causes increasing grain boundaries. Since the grain boundaries have energy, at the moment of impact of the crack on the grain boundaries, the crack energy is taken by the grain boundary [43, 44], which leads to increased fracture toughness and three-point flexural strength of this sample compared to the sintered sample at 1550 °C. Also, in the sintered sample at 1550 °C, due to the X-ray diffraction pattern and the presence of TiC phase resulting from Ti_3SiC_2 decomposition as the main peak and the dominance of this phase over the Ti_3SiC_2 phase in the sample, due to mismatch of thermal expansion coefficient between Ti_3SiC_2 and TiC, the fracture toughness of this sample is lower than that of the sintered sample at 1500 °C.

Table 2. Bulk and relative density as well as closed, apparent, and total porosity values of Ti_3SiC_2 specimens hot-pressed at two different temperatures.

Sample	Bulk density (g/cm^3)	Relative density (%)	Total porosity (%)	Apparent porosity (%)	Closed porosity (%)
Ti_3SiC_2 hot-pressed at 1500 °C	4.03	89	11	4.09	6.94
Ti_3SiC_2 hot-pressed at 1550 °C	4.44	98.08	1.92	1.52	0.41

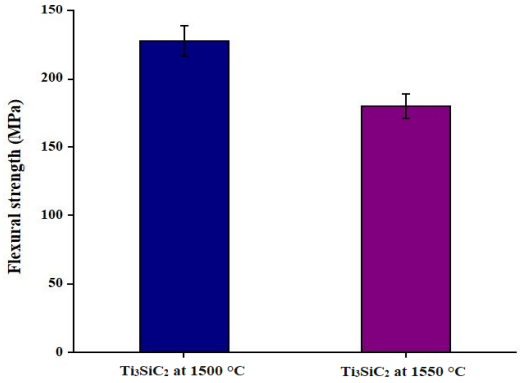

Fig. 4. Three-point flexural strength of Ti_3SiC_2 specimens hot-pressed at two different temperatures.

4. Conclusions

In summary, this project aims to determine the effect of different sintering temperatures with a difference of 50 °C on the hot-pressed monolithic Ti_3SiC_2 samples and the formed phases, microstructure and mechanical properties, to see at which sintering temperature the impurity phases disappear or reach their minimum state. Therefore, samples were sintered at 35 MPa under vacuum for 30 minutes at 1500 and 1550 °C by the hot-press method. According to the results obtained, the hot-pressed monolithic Ti_3SiC_2 sample at 1500 °C has good situation compared to the sintered sample at 1550 °C. SEM images of the cross-sectional area of the samples show that with increasing sintering temperature to 1550 °C, the microstructure of the sintered sample at 1550 °C compared to the sintered sample at 1500 °C due to the limited placement of TiC particles in the grain boundaries increased. Also, increasing the sintering temperature to 1550 °C causes the decomposition of Ti_3SiC_2 to TiC, which can be seen as the main peak in the X-ray diffraction pattern. This leads to an increase in the relative density of this sample compared to the sintered sample at 1500 °C.

On the other hand, the three-point flexural strength of the sintered sample at 1500 °C due to the TiC and $TiSi_2$ particles in the grain boundaries of Ti_3SiC_2 particles prevent the growth of these grains, compared to the sintered sample at 1550 °C has been increased. As a result, the fracture toughness of this sample (Ti_3SiC_2 at 1500 °C) is higher than that of the sintered Ti_3SiC_2 sample at 1550 °C due to the fine-grained structure and more grain boundaries. Also, the Vickers hardness of the sintered sample at 1500 °C is higher due to the fine-grained structure.

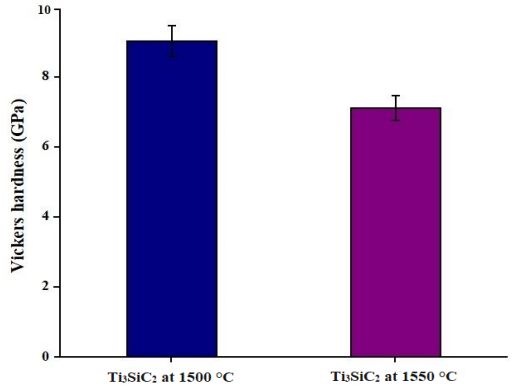

Fig. 5. Vickers hardness of Ti_3SiC_2 specimens hot-pressed at two different temperatures.

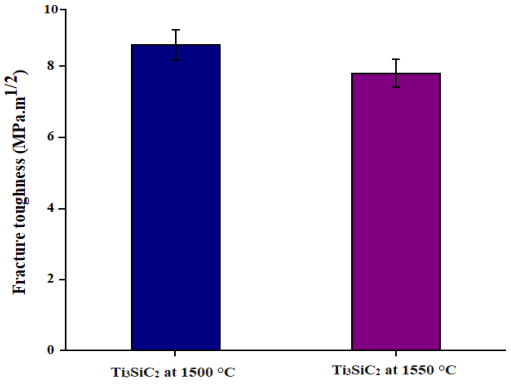

Fig. 6. Fracture toughness of Ti_3SiC_2 specimens hot-pressed at two different temperatures.

CRediT authorship contribution statement

Sheida Haji Amiri: Conceptualization, Investigation, Writing – original draft.

Nasser Pourmohammadie Vafa: Methodology, Project administration, Writing – review & editing.

Data availability

The data underlying this article will be shared on reasonable request to the corresponding author.

Declaration of competing interest

The authors declare no competing interests.

Funding and acknowledgment

The results of this paper is based on the master thesis of the first author, which was approved at the University of Tabriz. The authors would like to thank the Advanced Ceramic Research Gruop for its invaluable financial support.

References

[1] I. Kero, R. Tegman, M.-L. Antti, Effect of the amounts of silicon on the in situ synthesis of Ti3SiC2 based composites made from TiC/Si powder mixtures, Ceram. Int. 36 (2010) 375–379. https://doi.org/10.1016/j.ceramint.2009.07.029.

[2] J. Zeng, S. Ren, J. Lu, Phase Evolution of Ti3SiC2 Annealing in Vacuum at Elevated Temperatures, Int. J. Appl. Ceram. Technol. 10 (2013) 527–539. https://doi.org/10.1111/j.1744-7402.2012.02760.x.

[3] M.W. Barsoum, MAX Phases, Wiley-VCH Verlag GmbH & Co. KGaA, Weinheim, Germany. (2013). https://doi.org/10.1002/9783527654581.

[4] O. Dezellus, B. Gardiola, J. Andrieux, S. Lay, Experimental evidence of copper insertion in a crystallographic structure of Ti3SiC2 MAX phase, Scr. Mater. 104 (2015) 17–20. https://doi.org/10.1016/j.scriptamat.2015.03.015.

[5] P. Istomin, E. Istomina, A. Nadutkin, V. Grass, A. Leonov, et al., Fabrication of Ti3SiC2 and Ti4SiC3 MAX phase ceramics through reduction of TiO2 with SiC, Ceram. Int. 43 (2017) 16128–16135. https://doi.org/10.1016/j.ceramint.2017.08.180.

[6] N. Atazadeh, M. Saeedi Heydari, H.R. Baharvandi, N. Ehsani, Reviewing the effects of different additives on the synthesis of the

Ti3SiC2 MAX phase by mechanical alloying technique, Int. J. Refract. Met. Hard Mater. 61 (2016) 67–78. https://doi.org/10.1016/j.ijrmhm.2016.08.003.
[7] J.L. Huang, H.H. Lu, Microstructural and Mechanical Properties of Ti3SiC2 Composites, Key Eng. Mater. 403 (2008) 189–192. https://doi.org/10.4028/www.scientific.net/KEM.403.189.
[8] X. Liu, H. Zhang, Y. Jiang, Y. He, Characterization and application of porous Ti3SiC2 ceramic prepared through reactive synthesis, Mater. Des. 79 (2015). https://doi.org/10.1016/j.matdes.2015.03.061.
[9] H. Foratirad, H.R. Baharvandi, M. Ghanadi Maragheh, Synthesis of nanolayered Ti3SiC2 MAX phase via infiltration of porous TiC preform produced by the gelcasting process, Mater. Lett. 180 (2016) 219–222. https://doi.org/10.1016/j.matlet.2016.05.181.
[10] M. Zhu, R. Wang, C. Chen, H.B. Zhang, G.J. Zhang, Comparison of corrosion behavior of Ti3SiC2 and Ti3AlC2 in NaCl solutions with Ti, Ceram. Int. 43 (2017) 5708–5714. https://doi.org/10.1016/j.ceramint.2017.01.111.
[11] T. El-Raghy, M.W. Barsoum, Processing and Mechanical Properties of Ti3SiC2: I, Reaction Path and Microstructure Evolution, J. Am. Ceram. Soc. 82 (2004) 2849–2854. https://doi.org/10.1111/j.1151-2916.1999.tb02166.x.
[12] L. Shannahan, M.W. Barsoum, L. Lamberson, Dynamic fracture behavior of a MAX phase Ti3SiC2, Eng. Fract. Mech. 169 (2017) 54–66. https://doi.org/10.1016/j.engfracmech.2016.11.006.
[13] J. Zhang, L. Wang, W. Jiang, L. Chen, High temperature oxidation behavior and mechanism of Ti3SiC2–SiC nanocomposites in air, Compos. Sci. Technol. 68 (2008) 1531–1538. https://doi.org/10.1016/j.compscitech.2007.10.029.
[14] Y. Cai, X. Yin, H. Yin, Effects of SiC amount on phase compositions and properties of Ti3SiC2-based composites, J. Cent. South Univ. 22 (2015). https://doi.org/10.1007/s11771-015-2489-7.
[15] R. Radhakrishnan, J. Williams, M. Akinc, Synthesis and high-temperature stability of Ti3SiC2, J. Alloys Compd. 285 (1999) 85–88. https://doi.org/10.1016/S0925-8388(99)00003-1.
[16] S.-B. Li, J.-X. Xie, L.-T. Zhang, L.-F. Cheng, In situ synthesis of Ti3SiC2/SiC composite by displacement reaction of Si and TiC, Mater. Sci. Eng. A. 381 (2004) 51–56. https://doi.org/10.1016/j.msea.2004.03.046.
[17] S.-B. Li, J.-X. Xie, L.-T. Zhang, L.-F. Cheng, Mechanical properties and oxidation resistance of Ti3SiC2/SiC composite synthesized by in situ displacement reaction of Si and TiC, Mater. Lett. 57 (2003) 3048–3056. https://doi.org/10.1016/S0167-577X(02)01429-5.
[18] X. Tong, T. Okano, T. Iseki, T. Yano, Synthesis and high temperature mechanical properties of Ti3SiC2/SiC composite, J. Mater. Sci. 30 (1995). https://doi.org/10.1007/BF01209221.
[19] X. Guo, J. Wang, S. Yang, L. Gao, B. Qian, Preparation of Ti3SiC2 powders by the molten salt method, Mater. Lett. 111 (2013) 211–213. https://doi.org/10.1016/j.matlet.2013.08.077.
[20] J. Zhang, L. Wang, L. Shi, W. Jiang, L. Chen, Rapid fabrication of Ti3SiC2–SiC nanocomposite using the spark plasma sintering-reactive synthesis (SPS-RS) method, Scr. Mater. 56 (2007) 241–244. https://doi.org/10.1016/j.scriptamat.2006.09.029.
[21] H. Li, L.M. Peng, M. Gong, J.H. Zhao, L.H. He, C.Y. Guo, Preparation and characterization of Ti3SiC2 powder, Ceram. Int. 30 (2004) 2289–2294. https://doi.org/10.1016/j.ceramint.2004.01.009.
[22] L. Jaworska, Diamond Composites with TiC, SiC and Ti3SiC2 Bonding Phase, High Press. Res. 22 (2002) 531–533. https://doi.org/10.1080/08957950212434.
[23] M. Radovic, M.W. Barsoum, MAX phases: bridging the gap between metals and ceramics, Am. Ceram. Soc. Bull. 92 (2013) 20.
[24] L.H. Ho-Duc, T. El-Raghy, M.W. Barsoum, Synthesis and characterization of 0.3 Vf TiC–Ti3SiC2 and 0.3 Vf SiC–Ti3SiC2 composites, J. Alloys Compd. 350 (2003) 303–312. https://doi.org/10.1016/S0925-8388(02)00985-4.
[25] C.N. Ghosh, Synthesis and Tribological Characterization of In-situ Spark Plasma Sintered Ti3SiC2 and Ti3SiC2-TiC Composites, M.S. Thesis, Dhaka. (2009).
[26] J.-Y. Wang, Y.-C. Zhou, Polymorphism of Ti3SiC2 ceramic: First-principles investigations, Phys. Rev. B. 69 (2004) 144108. https://doi.org/10.1103/PhysRevB.69.144108.
[27] S. Li, G.-M. Song, Y. Zhou, A dense and fine-grained SiC/Ti3Si(Al)C2 composite and its high-temperature oxidation behavior, J. Eur. Ceram. Soc. 32 (2012) 3435–3444. https://doi.org/10.1016/j.jeurceramsoc.2012.04.029.
[28] H. Abderrazak, F. Turki, F. Schoenstein, M. Abdellaoui, N. Jouini, Influence of mechanical alloying on Ti3SiC2 formation via spark plasma sintering technique from Ti/SiC/C powders, Ceram. Int. 39 (2013) 5365–5372. https://doi.org/10.1016/j.ceramint.2012.12.042.
[29] M.Z. Sun, A. Murugaiah, T. Zhen, A. Zhou, M. Barsoum, Microstructure and mechanical properties of porous TiSiC, Acta Mater. 53 (2005). https://doi.org/10.1016/j.actamat.2005.05.034.
[30] E. Tabares, A. Jiménez-Morales, S.A. Tsipas, Study of the synthesis of MAX phase Ti3SiC2 powders by pressureless sintering, Bol. Soc. Esp. Ceram. 60 (2021). https://doi.org/10.1016/j.bsecv.2020.01.004.
[31] W. Zhou, B. Mei, J. Zhu, Fabrication of high-purity ternary carbide Ti3AlC2 by spark plasma sintering (SPS) technique, Ceram. Int. 33 (2007) 1399–1402. https://doi.org/10.1016/j.ceramint.2006.04.018.
[32] J. Nickl, K. Schweitzer, P. Luxenberg, Gasphasenabscheidung im system TiSiC, J. Less Common Met. 26 (1972) 335–353. https://doi.org/10.1016/0022-5088(72)90083-5.
[33] B.Y. Liang, S.Z. Jin, M.Z. Wang, Low-temperature fabrication of high purity Ti3SiC2, J. Alloys Compd. 460 (2008) 440–443. https://doi.org/10.1016/j.jallcom.2007.05.074.
[34] Y.Y. Zhu, S.S. Li, L. Li, A.G. Zhou, Synthesis and Decomposition of Ti3SiC2 under 1-5GPa at 1400°C, Key Eng. Mater. 602–603 (2014) 499–502. https://doi.org/10.4028/www.scientific.net/KEM.602-603.499.
[35] S. Haji Amiri, M. Ghassemi Kakroudi, T. Rabizadeh, M. Shahedi Asl, Characterization of hot-pressed Ti3SiC2–SiC composites, Int. J. Refract. Met. Hard Mater. 90 (2020) 105232. https://doi.org/10.1016/j.ijrmhm.2020.105232.
[36] S. Haji Amiri, M. Ghassemi Kakroudi, N. Pourmohammadie Vafa, M. Shahedi Asl, Synthesis and Sintering of Ti3SiC2–SiC Composites through Reactive Hot-Pressing of TiC and Si Precursors, Silicon. (2021). https://doi.org/10.1007/s12633-021-01207-z.
[37] T. El-Raghy, M.W. Barsoum, Diffusion kinetics of the carburization and silicidation of Ti3SiC2, J. Appl. Phys. 83 (1998) 112–119. https://doi.org/10.1063/1.366707.
[38] C. Racault, F. Langlais, R. Naslain, Solid-state synthesis and characterization of the ternary phase Ti3SiC2, J. Mater. Sci. 29 (1994) 3384–3392. https://doi.org/10.1007/BF00352037.
[39] H.O. Pierson, Handbook of Refractory Carbides & Nitrides: Properties, Characteristics, Processing and Applications, William Andrew Inc. (2013).
[40] A. Pourebrahim, H. Baharvandi, H. Foratirad, N. Ehsani, Low temperature synthesis of high-purity Ti3SiC2 via additional Si through spark plasma sintering, J. Alloys Compd. 789 (2019) 313–322. https://doi.org/10.1016/j.jallcom.2019.03.062.
[41] L.H. Ho-Duc, Synthesis and Characterization of the Properties of Ti3SiC2/SiC and Ti3SiC2/TiC Composites, Mater. Sci. Eng. (2002).
[42] R. Radhakrishnan, C.H. Henager, J.L. Brimhall, S.B. Bhaduri, Synthesis of Ti3SiC2SiC and TiSi2SiC composites using displacement reactions in the Ti-Si-C system, Scr. Mater. 34 (1996) 1809–1814. https://doi.org/10.1016/1359-6462(95)00663-X.
[43] S. Haghgooye Shafagh, S. Jafargholinejad, S. Javadian, Beneficial effect of low BN additive on densification and mechanical properties of hot-pressed ZrB2–SiC composites, Synth. Sinter. 1 (2021) 69–75. https://doi.org/10.53063/synsint.2021.1224.
[44] S. Jafargholinejad, S. Soleymani, Effects of carbon nano-additives on characteristics of TiC ceramics prepared by field-assisted sintering, Synth. Sinter. 1 (2021) 62–68. https://doi.org/10.53063/synsint.2021.1123.